Journal of Drug Delivery Science and Technology 98 (2024) 105895

Contents lists available at ScienceDirect

Journal of Drug Delivery Science and Technology

journal homepage: www.elsevier.com/locate/jddst

Naringenin-loaded poly(3-hydroxybutyrate-*co*-3-hydroxyvalerate)-based devices have an anti-inflammatory activity on microglia

G. Pecorini [a], A. Votta [b], G. Tiralongo [a,b], D. Volpi [a,b], E. Ferraro [b,**], D. Puppi [a,*]

[a] BIOLab Research Group, Department of Chemistry and Industrial Chemistry, University of Pisa, UdR INSTM Pisa, Via Moruzzi 13, 56124, Pisa, Italy
[b] Department of Biology, University of Pisa, Pisa, Italy

ARTICLE INFO

Keywords:
Polyhydroxyalkanoates
Naringenin
Ocular implants
Wet-spinning
Melt-spinning
Microglia

ABSTRACT

Retinal degenerative diseases, such as retinitis pigmentosa, represent a significant fraction of the burden of blindness. This kind of diseases involves the activation of microglial cells which causes neuroinflammation. Flavonoids, such as naringenin (Nar), are able to modulate the pro-inflammatory behavior of the microglia cells but their low bioavailability often hinders this activity. In this context, the aim of this research activity was the development of implantable drug delivery systems through Nar encapsulation into a polymeric matrix, as a valuable way to increase its bioavailability. For this purpose, a blend between microbial poly(3-hydroxybutyrate-*co*-3-hydroxyvaerate) (PHBV) and poly(D,L-lactide-*co*-glycolide (PLGA) was processed by means of two different fabrication techniques, i.e., melt-spinning and wet-spinning, to fabricate rods designed for ocular implantation. The two developed kinds of rod had different morphology and thermal properties, as demonstrated by scanning electron microscopy, thermogravimetric analysis, and differential scanning calorimetry. In addition, an increase in Nar concentration in the starting polymeric mixture (1–5 wt% respect to device weight) determined a higher drug encapsulation efficiency, with a resulting drug loading increasing from 0.5 to 3.5 % and from 0.4 to 4.4 % for melt- and wet-spun rods, respectively. A significant effect of processing technique and drug loading on the resulting release kinetics was also observed, with the devices loaded with a higher percentage of Nar reaching a 100 % cumulative drug release after 38 and 73 days in the case of wet- and melt-spun rods, respectively. In addition, the wet-spun rods showed a first order drug release kinetics while the melt-spun rods a zero order one. The bioactivity of the wet-spun rods was tested on lipopolysaccharide-activated BV2 as well as primary murine microglia cells, thus demonstrating the ability of the released flavonoid to favor cell maturation from a pro-inflammatory to an anti-inflammatory phenotype.

1. Introduction

Neurodegenerative diseases are a group of central nervous system pathologies, whose mechanism involves oxidative stress, mitochondrial dysfunction [1], alterations of the ubiquitin-proteasome system [2], and abnormal accumulation of misfolded proteins [3], resulting in cell death and damaging of nervous tissue. In particular, retinal degenerative diseases, such as retinitis pigmentosa, age-related macular degeneration, and diabetic retinopathy, make up a significant portion of the burden of blindness, being often untreatable and characterized by a progressive cell death within the neurosensory retina [4].

Microglial cells activation in a pro-inflammatory direction is necessary for cell signaling of phagocytosis functions, but the persistence of this condition and the lack of a phenotypic shift towards a reparative phenotype can have neurotoxic effects [5]. Indeed, this excessive and persistent activation of the pro-inflammatory state and a resulting chronic neuroinflammation have been linked to the underlying cause of most neurodegenerative diseases. In particular, in degenerative retinal diseases, the oxidative stress leads to photoreceptor degeneration and activation of microglia cells [6], causing a shift to a pro-inflammatory state necessary to eliminate damaged neurons. If the retinal microglia cells do not return to homeostasis, the resulting chronic inflammation can cause permanent vision loss.

Flavonoids have been reported to modulate the microglial responses, inhibiting the pro-inflammatory shift, and concurrently offset oxidative damage, protecting neurons in the retina [7]. They are polyphenolic

* Corresponding author.
** Corresponding author.
E-mail addresses: elisabetta.ferraro@unipi.it (E. Ferraro), dario.puppi@unipi.it (D. Puppi).

https://doi.org/10.1016/j.jddst.2024.105895
Received 25 March 2024; Received in revised form 12 June 2024; Accepted 14 June 2024
Available online 15 June 2024

compounds found in plants, with potential antioxidant, anti-inflammatory, immunomodulatory, cardioprotective, antimicrobial, and anticancer activity [8]. One of the main shortcomings in using flavonoids for therapeutic applications is represented by their low bioavailability, mainly caused by low water solubility and limited metabolic stability [9]. Indeed, oral treatment usually requires high doses of flavonoids to reach a therapeutic level at the site of action [10]. A possible solution to this issue is encapsulating the flavonoid into a polymeric matrix to develop oral formulations or implantable devices for *in situ* controlled drug release rate [11]. This approach is aimed at tuning critical parameters, such as drug biodistribution, half-life, and concentration, as well as total drug exposure of the target tissue over time [12]. Bioabsorbable polymers can be exploited in applications requiring the implantation of a device only temporary needed, in order to avoid a further surgical intervention for its removal. Bioabsorbable drug release systems can be made of synthetic polymers, such as poly (lactic acid) (PLA) [13], poly(lactic-*co*-glycolic acid) (PLGA) [14], and poly(ε-caprolactone) (PCL) [15], or natural polymers, such as chitosan [16], hyaluronic acid [17], collagen [18], and gelatin [19]. Polyhydroxyalkanoates (PHA)s are aliphatic polyesters obtained by microbial fermentation through industrial processes potentially complying with the concept of sustainable development. Their natural synthesis, cytocompatibility, and biodegradability, together with a thermoplastic behavior, make them unique candidates for advanced biomedical applications [20]. Among them, poly(3-hydroxybutyrate) (PHB) has a high degree of crystallization in the range 60–80 %, as a consequence of the high stereochemical regularity, resulting in a stiff and brittle mechanical behavior (elongation at break <10 %) with a high melting temperature (T_m) [21]. Its copolymerization to obtain poly(3-hydroxybutyrate-*co*-3-hydroxyvalerate) (PHBV) usually leads to a reduction of the crystallinity degree, being around 60 % throughout a wide range of composition from 0 to 95 % of 3-hydroxyvalerate units [22]. This results in increased flexibility and ductility (elongation at break up to 50 %), as well as a reduced T_m down to 130 °C, enhancing polymer processability through melt fabrication techniques [23]. In addition, blending with other polymers, including PCL, PLA, and PLGA, has been demonstrated to be a suitable means to improve PHBV processing properties. For instance, PLGA blending was recently exploited to develop PHBV-based solutions with optimized viscosity for fiber spinning approaches [24].

A clinical application of bioabsorbable polymers is based on their intravitreal injection, for instance in the form of cylindrical implants, sometimes referred to as rods or microrods, for localized ocular drug release [25]. As an example, Ozurdex® is an implantable dexamethasone-loaded depot made of PLGA (Allergan Inc., Irvine, CA), approved by Food and Drug Administration for the treatment of ocular macular edema [25]. These kinds of implants are designed to provide, at the same time, a minimally invasive implantation procedure and a long-term release (months) of the bioactive molecule. They are typically produced through cutting of continuous drug-loaded polymeric filaments obtained by extrusion. In particular, melt-spinning has been investigated by different articles for the fabrication of drug-loaded polymeric rods, thanks to its high versatility in terms of thermoplastic polymers processing into filaments with a controlled diameter [26]. Wet-spinning represents another technique widely exploited in the controlled drug release area thanks to its high versatility in terms of material selection, bioactive agent loading strategy, and fiber morphology tuning [27]. However, to the best of authors' knowledge, wet-spinning nor PHA have been investigated yet for drug-loaded intravitreal rod development.

In this context, this research activity was aimed at the design, fabrication, and characterization of PHBV/PLGA implantable devices for spatial- and time-controlled delivery of an anti-inflammatory molecule at a retinal level. The flavonoid naringenin (Nar, 5,7,4′-trihydroxyflavanone) was selected as loading bioactive compound, since it has shown encouraging results in terms of modulation of microglia phenotype *in vitro* [28]. The fabrication of PHBV/PLGA rods loaded with two different theoretical Nar concentrations (1 and 5 wt%) was investigated by employing either melt- or wet-spinning. Previous articles have reported that blending with other polymers can be exploited to optimize the processing properties of PHBV as melt or solution in an organic solvent. For instance, blending PHBV with poly(ε-caprolactone) (PCL), a biodegradable polyester with a low T_m (around 60 °C), was proven to be an effective strategy for the production of scaffolds by fused deposition modeling [29]. Since neither melt-spinning nor wet-spinning of PHBV/PLGA blends have not been reported in the literature yet, the here described manufacturing processes were proposed as innovative approaches aimed at overcoming the limited processability of PHBV. Encapsulation efficiency (EE), drug loading (DL), and drug release kinetics in phosphate buffered saline (PBS) of the fabricated rods were determined using UV spectroscopy. Rods morphological characterization was carried out through scanning electron microscopy (SEM) analysis, while their thermal characterization by differential scanning calorimetry (DSC). An *in vitro* biological evaluation was carried out employing the BV2 murine microglia cell line, as well as primary murine microglia cells. Cell viability was assessed via indirect immunofluorescence, while gene expression related to markers associated with the two states of microglia activation was verified by real time reverse-transcription quantitative polymerase chain reaction (RT-qPCR).

2. Materials and methods

2.1. Materials

Naringenin (Nar, T_m = 250–251 °C, ethanol solubility = 48 mg/mL, water solubility = 10 μg/mL, LogP = 3.19 [30]) was bought from Sigma Aldrich (Milan, Italy) and used without further purification. Poly (3-hydroxybutyrate-*co*-3-hydroxyvalerate) (PHBV, M_n = 152 kDa, 19 mol% hydroxyvalerate) was provided by Biocycle (Serrana, Brazil). Poly (D,L-lactide-*co*-glycolide) with a lactide/glycolide 50:50 molar ratio (PLGA50:50, M_n = 207 kDa) and with a 75:25 molar ratio (PLGA75:25, M_n = 207 kDa) were bought from Vornia Biomaterials (Dublin, Ireland). Phosphate buffer saline (PBS) was prepared by dissolving 8 g of NaCl, 0.2 g of KCl, 0.2 g of KH_2PO_4, 1.44 g of $Na_2HPO_4{\cdot}2H_2O$ and 1 g of NaN_3 in 1 L of deionized water and adjusting the pH to 7.4. Chloroform ($CHCl_3$) and absolute ethanol (EtOH) were provided by Carlo Erba (Milan, Italy) and employed without further purification.

2.2. Melt-spinning

Given amounts of PHBV, PLGA50:50, and Nar were physically mixed using a mortar. In particular, three different physical mixtures differing for Nar concentration (0, 1, and 5 wt%) were prepared by keeping constant a 50:50 wt% PHBV/PLGA ratio (Table 1). The physical mixtures were left in a desiccator for 24 h before processing, then 20 g of each sample were processed employing a single screw melt-extruder (Composer 350 Filament Maker 3Devo, Utrecht, Netherland). The polymeric material was fed into a hopper and forced through a screw into four sections kept at different temperatures (175, 185, 190, 170 °C) to allow material melting and homogenization. The material was finally extruded through a nozzle and the obtained filament cooled down by a forced-air cooling process and then wrapped around a winder at room temperature. The resulting filament was finally cut to the final rod

Table 1
Composition of the physical mixtures employed for melt-spinning (MS) and wet-spinning (WS).

Rod	PHBV [wt%]	PLGA [wt%]	Nar [wt%]
MS-Nar0/WS-Nar0	50.0	50.0	0
MS-Nar1/WS-Nar1	49.5	49.5	1
MS-Nar5/WS-Nar5	47.5	47.5	5

length employing a scalpel blade.

2.3. Wet-spinning

PHBV was suspended in $CHCl_3$ at 35 °C for 7 h, then the desired amount of Nar was added to the suspension and the obtained mixture was left under stirring at room temperature overnight. PLGA75:25 was finally dissolved in the prepared suspension under magnetic stirring for 4 h at 35 °C. Like in the case of melt-spinning, mixtures containing different amounts of Nar were prepared. The polymeric matrix was made of PHBV and PLGA in a 50/50 % w/w ratio and the total concentration of the three components in $CHCl_3$ was 20 % w/v (Table 1). The prepared polymeric mixture was loaded in a glass syringe equipped with a blunt needle with an inner diameter of 0.41 mm (22 gauge). Wet-spinning was carried out using a customized apparatus constituted by a translating syringe pump and a rotating mandrel, both of them controlled by a dedicated software. The mandrel as well as the tip of the needle were immersed in a 160 mL EtOH bath and the coagulating fiber was wrapped around the rotating mandrel. At the end of the wet-spinning process, the wrapped-filament was collected from the coagulation bath, left overnight under a fume hood, and vacuum dried for 8 h. After that, the filament was ground into a mortar with liquid nitrogen.

2.4. Films preparation

For the preparation of films by solvent casting to be used in encapsulation efficiency measurements (see section 2.7), the desired amount of Nar and polymers or Nar-loaded rods were dissolved in $CHCl_3$ (1 % w/v) under magnetic stirring at 35 °C for 6 h. The obtained mixture was then cast on a Petri dish that was maintained overnight in an environment near to $CHCl_3$ saturation condition, and the resulting film was kept under a fume hood for 24 h and finally vacuum dried for 8 h.

2.5. Scanning electron microscopy (SEM)

Rods external surface and transversal cross-section, the latter obtained by fragile fracture in liquid nitrogen, were observed through scanning electron microscopy (SEM, JEOL JSM 300, Tokyo, Japan). The rods length and diameter were measured by Image J 1.43u software on micrographs with 100 × magnification. Data were calculated over 3 measurements per scaffold.

2.6. Thermal characterization

Thermogravimetric analysis (TGA) was performed using a TGA Q500 instrument (TA Instruments, Milan, Italy) in the temperature range 30–700 °C, at a heating rate of 10 °C/min, and under an air flow of 60 mL/min. Scaffolds' thermal degradation was evaluated by analyzing weight and derivative weight profiles as a function of temperature.

Differential scanning calorimetry (DSC) analysis was performed using a Mettler DSC-822 instrument (Mettler Toledo, Milan, Italy). The samples were subjected to two heating cycles in the range −20 to 200 °C at a heating rate of 10 °C/min, separated by a cooling cycle at a rate of −20 °C/min and by isothermal steps, the first one at 200 °C and the second one at −20 °C. The analyses were carried out under a nitrogen flow of 80 mL/min. By analyzing the thermograms relevant to the first and second heating cycles, polymer glass transition temperature (T_g) was obtained at the inflection point, melting temperature (T_m) as the maximum of the melting peak, and crystallinity (χ) as the ratio between the sample melting enthalpy (calculated as the area under the melting peak) and the melting enthalpy associated to 100 % crystalline PHBV (109 J/g [31]). All thermal characterization tests were carried out by analyzing three sample replicates.

2.7. Evaluation of encapsulation efficiency (EE)

The solvent cast films, prepared as described in Section 2.4, were kept in 40 mL of EtOH into a round bottom flask equipped with a reflux condenser, at 80 °C for 6 h under magnetic stirring. The EtOH-rich extract phase was analyzed after filtration employing a UV/Vis V-530 spectrophotometer (Jasco International Co., Ltd., Japan) with quartz cuvettes. A calibration curve was employed to obtain Nar concentration by analyzing data relevant to absorbance at 289 nm. Drug encapsulation efficiency (EE) and drug loading (DL) were calculated using Eq. (1) and Eq. (2), respectively.

$$\text{EE}\,[\%] = \frac{\text{mg of active agent actually encapsulated}}{\text{mg of active agent theoretically encapsulated}} \text{ x } 100 \qquad \text{Eq. 1}$$

$$\text{DL}\,[\%] = \frac{\text{mg of active agent actually encapsulated}}{\text{mg of device}} \text{ x } 100 \qquad \text{Eq. 2}$$

All the analyses were carried out on three sample replicates.

2.8. Nar release kinetics

To determine the release kinetics of the developed devices, 355 mg of rods were incubated in 16 or 48 mL of PBS in the case of rods loaded with a theoretical Nar concentration of 1 or 5 wt%, respectively, on an orbital shaker at 37 °C. At prefixed time intervals, 0.5 mL of the incubation medium were collected from each bottle and replaced with fresh PBS. The collected samples were analyzed by means of UV spectroscopy using a V-530 spectrophotometer (Jasco International Co., Ltd., Japan) and quartz cuvettes. The absorbance peak at 321 nm was used to determine the concentration of the drug in PBS and checked against a calibration curve. All the analyses were carried out on three sample replicates.

2.9. Cell cultures

Murine BV2 microglia cells were grown in Dulbecco's Modified Eagle Medium (DMEM), containing GlutaMAX, Pyruvate, 4.5 g/L of D-Glucose, 5 % v/v Fetal Bovine Serum, and 1 % v/v Penicillin/Streptomycin at 37 °C in a 95 % O_2 and 5 % CO_2 humidified chamber. All reagents for media preparation were from Thermo Fisher Scientific (Monza, Italy). Microglial primary cultures were derived from cerebral cortices of post-natal day 0–2 (p0–p2) wt mice. Following the removal of meninges, cortical tissue was dissected and placed in cold HBSS (Hank's Balanced Salt Solution) supplemented with 10 mM HEPES (Gibco), devoid of Ca^{2+} and Mg^{2+}. The cortices were then minced into small fragments and enzymatically digested using 0.25 % trypsin and 0.01 % DNaseI. Following dissociation and filtration through 70-mm filters, cells were suspended in high glucose DMEM-F12 supplemented with Glutamax, 10 % FBS, and 1 % penicillin/streptomycin. After 9–11 days, cultures were shaked for 2 h at 37 °C to detach and collect microglia cells.

2.10. Cell treatments

Two different experiments have been carried out in order to evaluate the anti-inflammatory activity of wet-spinning rods loaded with a theoretical Nar concentration of 5 % w/w (WS-Nar5 rods) and using unloaded rods as reference (WS-Nar0). In the first type of experiments rods (28,8 mg calculated considering the rods release kinetics, in order to reach a 60 μM concentration of Nar in 24 h) were incubated in 10 mL DMEM + P/S and placed on a mechanical wheel at 37 °C for 24 h. 6-Well or 12-well plates were used and 11×10^4 or 4.4×10^4 cells/well were plated in 2/1 mL of complete medium. After 24 h of incubation, DMEM containing WS-PPNar5 and WS-PPNar0 (used as control) were centrifuged at 300 RCF for 5 min to remove the device. The supernatant, which contained only DMEM + P/S and Nar released by the device, was used to replace the cell medium in plates with the subsequent addition of

3 % v/v FBS. After 6 h, the inflammatory activity of microglial cells was stimulated using 100 ng/mL lipopolysaccharide (LPS). 18 h after the administration of the inflammatory stimulus (LPS), the experiment was stopped, the culture medium was removed and the extraction of RNA was performed. In the second type of experiments, 28,8 mg of WS-Nar5 and 28,8 mg of WS-Nar0 were placed in medium for 24 h, as described for the previous experiment. After that, the medium containing the device was used to replace cell culture medium on cells. After 6 h, LPS was added to the medium and after 18 h the experiment was stopped.

2.11. Real-time RT-qPCR

The RNA isolation from BV2 and primary microglia cells treated as above reported was performed by using the Invitrogen™ TRIzol™ Reagent following the manufacturer's instructions. The cDNA was synthesized by using 1–3 μg RNA and the GoScript Reverse Transcription System (Promega) with Random Primers. Comparative qPCR was performed with the SensiMix SYBR No-ROX (Meridian Bioscience) by using the QuantStudio 3 (Applied Biosystem by Thermo Fisher Scientific). Data were normalized to 18S gene and analyzed by using the $2-\Delta\Delta CT$ method. The sequences of the used primers are reported in Table 2. All reactions were performed in duplicate. Data shown are the mean ± SE from n = 6 experiments each performed in triplicate.

2.12. Fluorescence microscopy

For immunofluorescence analysis, cells were fixed with 4 % w/v paraformaldehyde (PFA) solution, with DPBS, permeabilized 0.4 % v/v Triton-X-100 for 5 min, and blocked with 2 % v/v horse serum (HS) for 30 min.

After the blocking step, cells were incubated overnight at 4 °C with antibodies against cytochrome *c* (BD Biosciences; 556432) and cleaved caspase-3 (Sigma-Aldrich; ab3623). Samples were then washed and incubated for 1 h with a secondary antibody (1:500; Thermo Fisher Scientific) at room temperature. Nuclei were counterstained with 4',6 diamidino-2-phenylindole (DAPI, Thermo Fisher Scientific), washed with PBS and the coverslip was mounted on a slide in Aqueous Mounting solution (Sigma-Aldrich, USA). The images were acquired with a Nikon Eclipse Ti fluorescence microscope equipped with the software NIS-Elements AR 5.11.03 (Nikon Corporation). Data shown are representative of n = 3 experiments.

2.13. MTS

MTS Cell Titer 96AQueous One solution cell proliferation assay was performed according to the supplier's instructions (Promega, Madison, WI). The MTS [3-(4,5-dimethylthiazol-2-yl)-5-(3-carboxymethoxyphenyl)-2-(4-sulfophenyl)-2H-tetrazolium, inner salt] tetrazolium compound is bioreduced into a colored formazan product by NADPH or NADH produced by dehydrogenase enzymes in metabolically active cells. In order to be sure to perform the assay on the whole cell population including the dead cells, also the incubation medium was analyzed. To this purpose, sedimentation of floating cell-rods from the incubation medium was allowed (30 s on the bench) and supernatants were centrifuged at high speed (500 g 10 min) to obtain a pellet. In parallel, adherent cells were detached from the dish and added to the floating cell-rods of the incubation medium previously sedimented, centrifuged (300 g, 5 min), washed and incubated with trypsin, washed two times and left 30 s on the bench to allow sedimentation of rods which were removed. Cells were then centrifuged (300 g, 5 min) and the obtained pellet was added to the one previously obtained from the incubation medium. The control cells underwent exactly the same procedure as the rod-incubated ones. Cells were counted in order to perform the MTS assay on the same number of control and rod-incubated cells. Cells were plated in triplicate in 96-well plates at a density of $1{\cdot}10^4$ cells per well. Cell Titer 96Aqueous One solution was added to each well for 2 h and 30 min at 37 °C, and the light absorbance at 490 nm was recorded using a 96-well plate reader (VERSAmax microplate reader). Values were normalized to blank controls (culture medium and tetrazolium without cells) whose signal represents the absorbance background at 490 nm. Data shown are the mean ± SE from n = 4 experiments each performed in triplicate.

Table 2
Primer sequences used for RT-qPCR.

Primer	Forward sequence	Reverse sequence
Actin	TTGAATCCTGTGGCATCCATGAAAC	TTAAACGCAGCTCAGTAACA
IL-1β	GACCTTCCATGAGGACA	TCCATTGAGGTGGAGAGCTT
CCL2	AGGTCCCTGTCATGCTTCT	CTCCAGCCTACTTGGGA
iNOS	GGGTGGCCTCGAATTCCCAG	CCATCCTTCGGCCCACTTCC
CD206	GACGGACGAGGAGTTCATTATAC	GTTGGAGAGATAGGCACAGAAG

2.14. Statistical analysis

Data were reported as mean ± standard deviation or mean ± standard error, where appropriate. Data sets were analyzed with pertinent statistical testing (*t*-test or one-way ANOVA followed by Tukey HSD test). The differences were considered significant for a p value < 0.05.

3. Results and discussion

3.1. Rods manufacturing

Experimental protocols for the fabrication of implantable rods made of a PHBV-PLGA blend (1:1 wt ratio) and loaded with two different theoretical Nar concentrations (1 or 5 wt%) were optimized by employing either melt- or wet-spinning.

3.1.1. Rods fabrication by melt-spinning

This manufacturing approach involved processing by melt extrusion a PHBV-PLGA mixture containing Nar to obtain rods with a diameter of around 0.5 mm, suitable for intravitreal implantation [32]. In particular, PHBV, PLGA50:50, and Nar powders were mixed using a mortar and the resulting physical mixture was fed to a single screw extruder to produce a continuous filament, collected by means of a rotating winder and finally cut into rods with a length of around 6 mm (Fig. 1A). Mortar grinding was selected as a suitable pre-extrusion physical mixing technique to minimize the use of the investigated polymers and bioactive agent, as well as the risks of contamination. The homogeneity of the physical blend after mortar grinding was visually checked before extrusion. In addition, Nar loading was evaluated by analyzing rods obtained at different extrusion times, achieving a low standard deviation (see section 3.4), which suggested that the drug was quite uniformly distributed along the filament. Indeed, melt extrusion is a technique commonly employed for the preparation of polymeric blends as well as for the efficient and homogenous dispersion of additives into a polymeric matrix [33]. By optimizing different processing parameters, including the temperature of the four different extruder zones (170, 190, 185, and 175 °C) and the screw rotation rate (2 rpm), melt-spun rods unloaded or loaded with a theoretical Nar concentration of 1 or 5 wt%, referred to as MS-Nar0, MS-Nar1, and MS-Nar5, respectively (Table 1), were successfully fabricated.

PHBV has a relatively narrow processing temperature range, between its T_m and degradation temperature (~200 °C), as well as low melt viscosity and elasticity, limiting its processing by melt-extrusion [34]. However, blending with other polymers or low molecular weight additives can improve its workability in the molten state. In particular, PHBV blending with PLGA50:50, a polymer matrix of clinically employed ocular implants [32], was effectively exploited to achieve a uniform and continuous extrusion of the polymeric mixture. Attempts to process by melt-spinning PHBV blends with PLGA75:25, the latter used

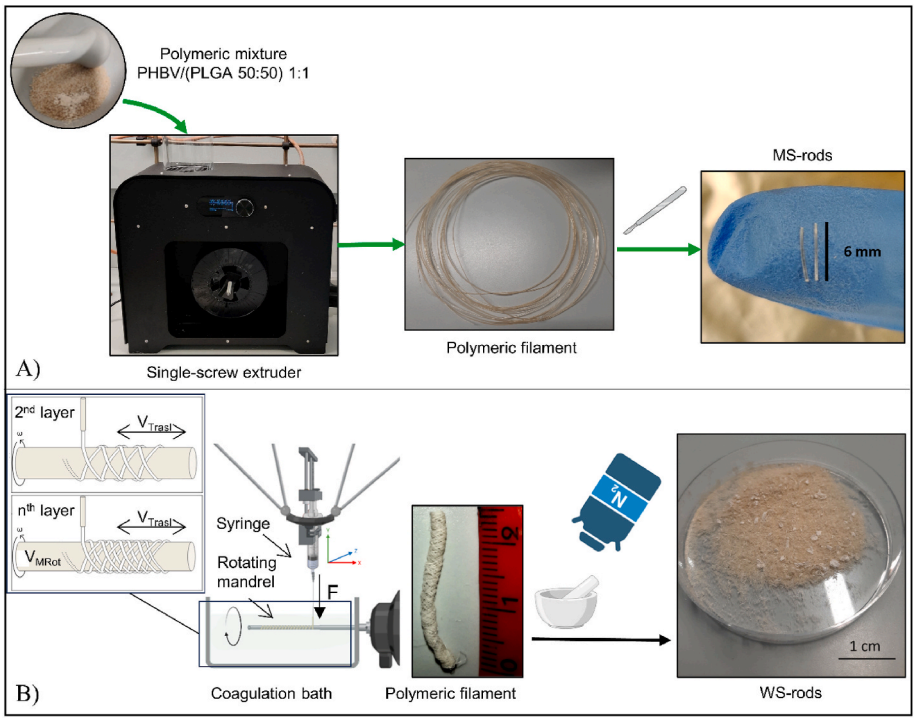

Fig. 1. Rods manufacturing. Schematic representation of the processes for Nar-loaded PHBV/PLGA rods fabrication through A) melt-spinning, or B) wet-spinning.

instead in the case of optimized wet-spinning (see Section 3.1.2), were not successful likely due to a high polymeric mixture viscosity.

3.1.2. Rods fabrication by wet-spinning

Polymeric mixtures to be processed by wet-spinning were obtained through addition under magnetic stirring of PHBV and PLGA75:25 to $CHCl_3$, since PLGA can be completely solubilized in this solvent while PHBV and Nar can form a stable suspension [35]. In particular, Nar was suspended in $CHCl_3$ before the addition of PLGA, because the solubilization of the latter led to a significant increase of mixture viscosity. PLGA75:25 was selected for this manufacturing process because it resulted in a more viscous solution, in comparison to PLGA50:50, suitable for optimized welt-spinning.

Filament wet-spinning was carried through extrusion of a PHBV/PLGA/$CHCl_3$ mixture, possibly containing Nar, through a needle whose tip was immersed in an EtOH bath at room temperature. This solvent/non-solvent system was selected to exploit the high miscibility between the two components and the optimized coagulating effect of EtOH [24]. The polymeric fiber deriving from the non-solvent-induced phase inversion process governing the solidification process was wrapped around a rotating metal mandrel, immersed in the EtOH bath, whose movement was controlled by means of a dedicated software (Fig. 1B) [36]. The most influent optimized processing parameters were the extrusion flow rate (F = 2 mL/h), the translation speed of the needle (V_{trasl} = 240 mm/min), the rotational velocity of the fiber collector (V_{rot} = 2 rpm), the distance on the Y axis between the needle tip and the collector (d_y = 5 mm), and the distance on the Z axis between the needle and the collector (d_z = 1 mm). Since the wrapped filament was welded at the contact points forming a tubular cohesive assembly, it was not possible to unwrap and then cut it to obtain fragments with a length comparable to that of melt-spun rods (≈6 mm). Therefore, the obtained tubular samples were ground into a mortar, using liquid nitrogen to make the material brittle and facilitating the process, obtaining rods of smaller dimensions compared to those of melt-spun rods.

Wet-spun rods unloaded and loaded with a theoretical Nar concentration of 1 or 5 wt%, referred to as WS-Nar0, WS-Nar1, and WS-Nar5, respectively (Table 1), were successfully fabricated by means of this manufacturing process.

3.2. Scanning electron microscopy (SEM) analysis

Micrographs at different magnifications relevant to both the external surface and the transversal cross-section of the two kinds of developed rods were obtained by SEM analysis.

Micrographs of unloaded melt-spun rods (MS-Nar0) or those loaded with a theoretical Nar concentration of 1 or 5 wt% (MS-Nar1 and MS-Nar5, respectively) are reported in Fig. 2. These rods had a uniform external surface morphology, characterized by a dense and continuous polymeric matrix. Although there were no detectable differences between MS-Nar0 and MS-Nar1, a rough topography could be appreciated on the external surface of the MS-Nar5 rods, likely due to adsorbed Nar crystal microparticles.

A comparative analysis of micrographs relevant to melt-spun rods transversal cross-section (Fig. 2A) highlighted a peculiar morphology in the case of Nar-loaded samples, related to the presence of two different polymeric phases. Indeed, this blend upon extrusion can lead to the formation of a continuous PHBV matrix in which PLGA fibrils are dispersed, due to shear forces acting on the melt material [24]. This particular morphology was more evident in MS-Nar1 samples, suggesting that the presence of Nar at a low concentration can favor this phase segregation by causing a slower polymer solidification that allow polymer chains to organize into a biphasic semicrystalline (PHBV) and amorphous (PLGA) morphology, typical of immiscible polymers [37]. However, further tests should be carried out to evaluate this aspect and confirm the possible interaction of Nar with the PHBV-PLGA polymeric blend, e.g., through hydrogen bonding or as nucleating agent for crystallization, as previously shown for other crystalline additives [38].

SEM micrographs of unloaded wet-spun rods (WS-Nar0), as well as those of wet-spun rods loaded with a theoretical Nar concentration of 1 or 5 wt% (WS-Nar1 and WS-Nar5, respectively) are reported in Fig. 2B. These rods were characterized by variable sizes (1–2 mm long and a diameter of approximately 150–200 μm), smaller than those of melt-spun rods, as a consequence of the different solidification process and the manual milling procedure. The geometry of some samples was

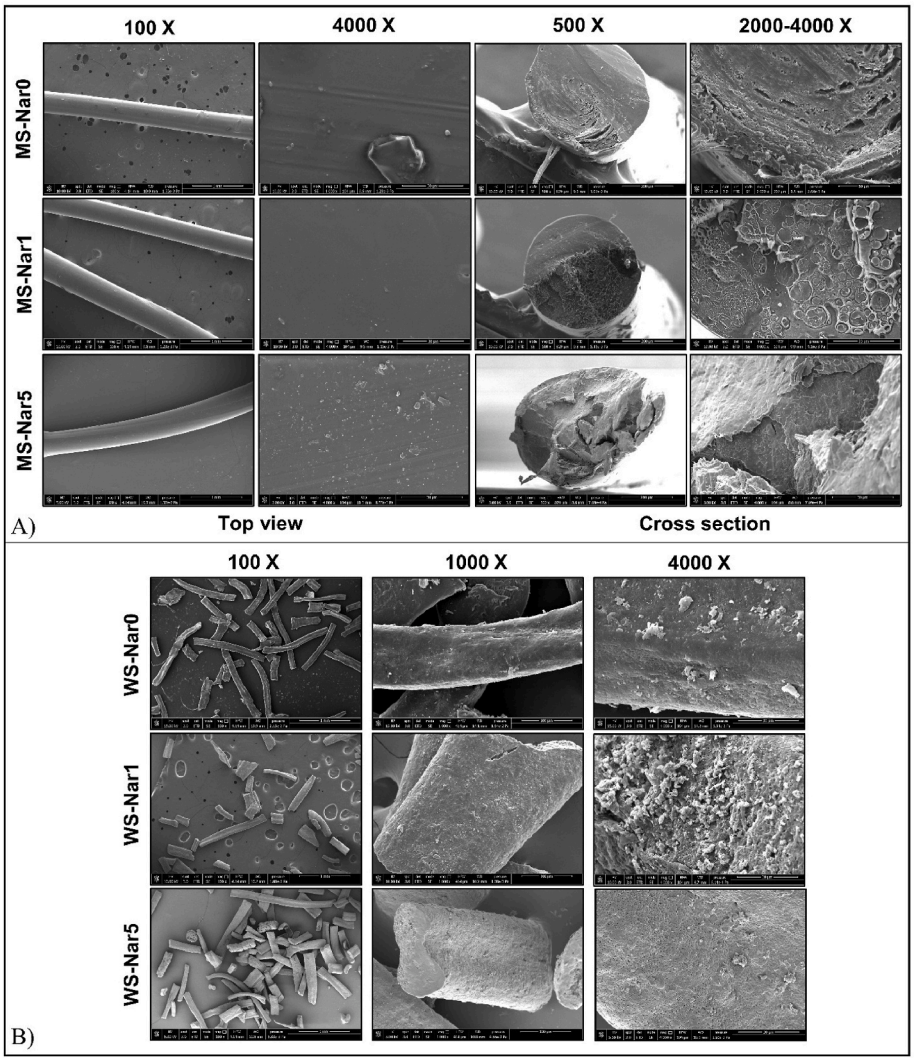

Fig. 2. SEM analysis. Micrographs at different magnifications of A) melt-spun and B) wet-spun rods unloaded or loaded with different concentrations of Nar.

approximately cylindrical, while an irregular shape was observed in other cases. High magnification analysis highlighted that the rods surface was characterized by a diffuse roughness, differently to what observed in the case of melt-spun rods characterized by a more uniform surface, while the presence of the flavonoid led to an increase in surface roughness and the presence of micropores. Also in this case, an effect of Nar on polymeric material solidifcation process can be hypothesized, since a large body of literature has demonstrated the effect of additives in the starting solution on non solvent-induced phase separation kinetics and the resulting matrix morphology [27].

3.3. Thermal characterization

A thermogravimetric analysis (TGA) in air was carried out in order to assess the thermal stability of Nar and the polymers employed for melt-spinning (Fig. 3A and B). PHBV and PLGA50:50 thermograms were characterized by a single weight loss event relevant to polymer thermal degradation, with a maximum rate (T_{max}) at 278 °C and 347 °C, respectively, while Nar thermogram showed two degradation events, the first one with a T_{max} of 313 °C and the other one T_{max} of 540 °C. Onset temperatures (T_{onset}) of the three analyzed samples are all above the temperatures employed for melt-spinning ($T \leq 190$ °C) indicating that they were suitable for this processing approach.

Nar DSC thermogram (Fig. 3C) was characterized by a single endothermic peak between 240 and 260 °C and centered at around 255 °C, corresponding to drug crystals melting. Considering that melt-spinning was carried out in the temperature range 170–190 °C, it is possible to speculate that Nar remained in a crystalline state during processing.

DSC thermograms relevant to the first heating cycle for both typologies of rod (Fig. 4A–C) showed characteristic thermal transitions of the two polymers: an endothermic peak centered at about 164 °C related to PHBV crystallites melting, and an inflection point at around 50 °C corresponding to PLGA glass transition.

PHBV T_m and crystallinity degree (χ^*), the latter normalized in relationship to PHBV weight percentage in the polymeric matrix, were significantly reduced both after melt- and wet-spinning (Tables S1 and S2). This result can be related to an effect of PLGA on the PHBV crystallization process starting from a melt or an organic solvent solution which is then coagulated in a non-solvent [39]. In some cases, a significant increase in PLGA T_g after processing was also detected, a phenomenon already observed in previous studies on blends between immiscible polymers, like in this case, attributable to the chain ends tendency to converge at the interphase [40]. PLGA T_g in wet-spun rods, as well as PHBV T_g in melt-spun rods, were significantly decreased upon Nar loading. Polymer plasticization typically results in increased flexibility of drug delivery devices favoring their adaptation to the site of injection [41]. In addition, depending on the hydrophilic/hydrophobic balance of the polymeric matrix, a reduction of polymer T_g below the physiological temperature can also lead to an increased burst release, like for instance in the case of aliphatic polyester colloidal suspensions

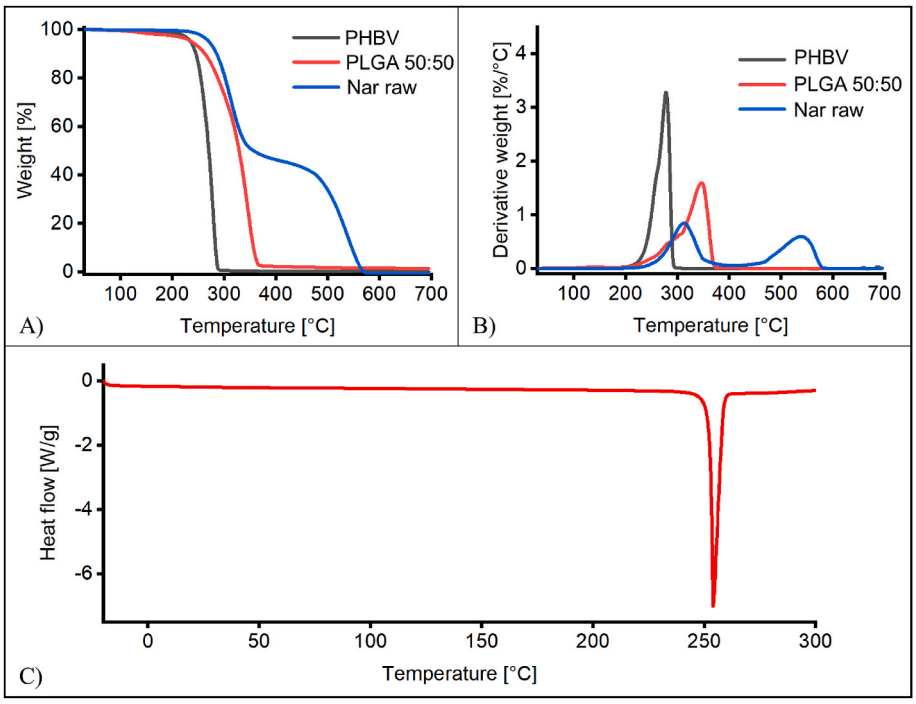

Fig. 3. Thermal analysis of raw materials. TGA in air: thermograms relevant to A) weight and B) derivative weight vs. temperature of the materials employed for melt-spun rods fabrication; C) differential scanning calorimetry (DSC) thermogram of Nar.

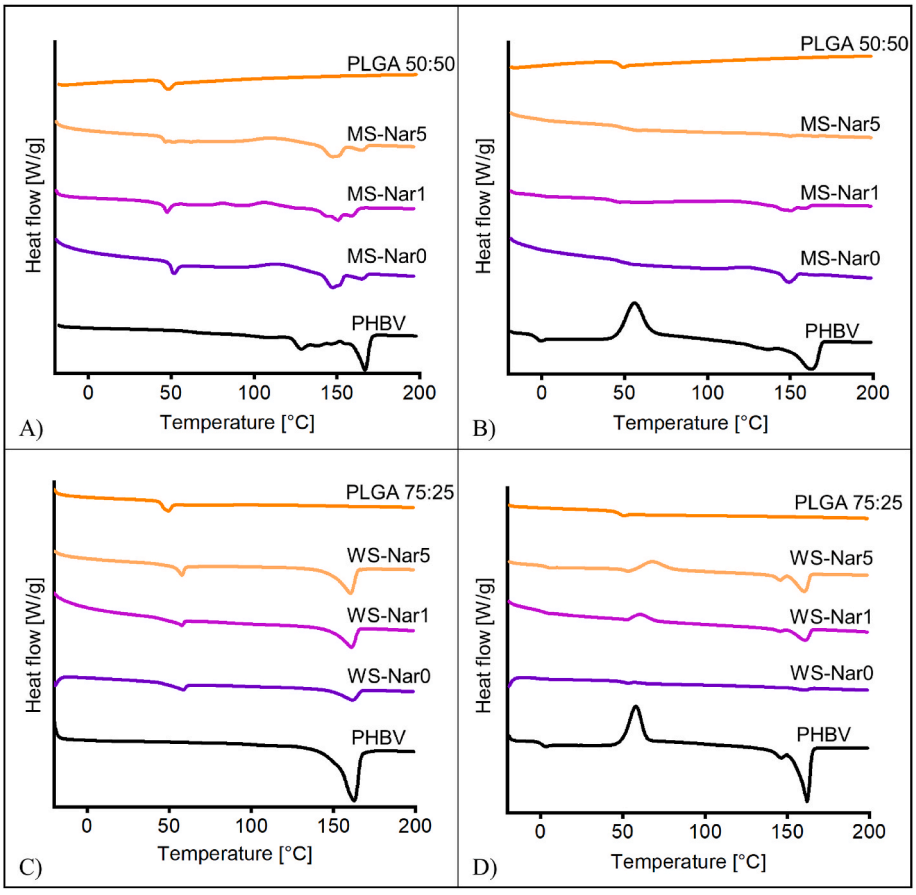

Fig. 4. DSC analysis of rods. Thermograms relevant to A) first and B) second heating scan of melt-spun rods, C) first and D) second heating scan of wet-spun rods.

[42]. Melt-spun rods thermograms also showed one or two overlapped exothermic peaks just before the melting event, related to cold crystallization of PHBV. As a result of the high PHBV χ^*, it was not possible to observe in the first heating scan its glass transition for every analyzed samples.

Instead, in the second heating scan thermograms (Fig. 4B–D) the PHBV glass transition at around 0 °C was evident in the case of some Nar-loaded samples, as a consequence of the relatively high cooling rate of the previous cycle (−20 °C/min), which kinetically disadvantaged polymer crystallization. For the same reason, an exothermic peak at around 60 °C relevant to PHBV cold crystallization, overlapped with PLGA glass transition inflection point, was detected also for Nar-loaded wet-spun samples, with a significant larger cold crystallization enthalpy (ΔH_{cc}) in the case of WS-Nar5. In the case of the second heating scan of MS-Nar0 and MS-Nar1, a shift of cold crystallization peak at higher temperatures in comparison to that of raw PHBV was evident, while in the case of MS-Nar5 PHBV cold crystallization was suppressed. A concentration-dependent significant effect of Nar loading on PHBV χ^* was also observed during the first and second heating cycle, such as in the in the case of MS-Nar5 showing a higher value than the unloaded MS-Nar0 sample in the first cycle.

Summarizing, the obtained results demonstrated that Nar loading affected the PHBV crystallization process both during rods manufacturing and DSC heating/cooling scans. This evidence corroborates the hypothesis that Nar loading may have had an effect on polymer solidification kinetics, influencing the resulting surface roughness and biphasic morphology, as observed during SEM analysis. In addition, these results can have a significant impact from an application point of view, since the well-known effect of polymer crystallinity on material wettability and biodegradation, as well as drug diffusivity through the polymeric matrix, which are parameters of paramount importance to understand the resulting drug release kinetics [43].

3.4. Encapsulation efficiency (EE) and drug loading (DL)

The evaluation of Nar encapsulation efficiency (EE) and drug loading (DL) in the polymeric matrix was carried out first through dissolution of the rods in $CHCl_3$ to prepare a film by solvent casting, in order to avoid any effect of polymer matrix morphology on this quantitative analysis. In order to evaluate the efficiency of this extraction method, solvent cast films were also prepared starting from known amounts of polymers and Nar, using the starting weight percentages employed for rods manufacturing. Nar was then selectively leached from the different kinds of the prepared films employing EtOH, and the extracts were analyzed by means of UV spectroscopy (Fig. 5A). The leaching method was optimized in terms of extraction solvent, temperature, and time. Among the tested solvents (i.e., EtOH, isopropanol and hexane), EtOH was selected because it is able to selectively dissolve Nar at high concentrations and resulted in the highest extraction efficiency. The optimized extraction temperature was 60 °C, since lower temperatures determined slower Nar dissolution, while higher temperatures led to lower extraction efficiency probably due to Nar degradation. Finally, the optimized extraction time resulted to be 6 h, since longer times did not allow to further increase the extraction efficiency [44].

Table 3
Data relevant to the encapsulation efficiency (EE), drug loading (L) and fitting data of the release kinetics curves of the developed rods.

	EE [%]	DL [%]	Function	R-squared
MS-Nar1	47 ± 9*,**	0.5 ± 0.1*,**	$y = ax + b$	0.99678
MS-Nar5	69 ± 9*,°	3.5 ± 0.5*,°	$y = y_0 + Ae^{kx}$	0.98513
WS-Nar1	44 ± 5°	0.4 ± 0.1°	$y = y_0 + Ae^{kx}$	0.96423
WS-Nar5	87 ± 4**	4.4 ± 0.1**	$y = y_0 + Ae^{kx}$	0.75009

Data are reported as mean ± standard deviation (n = 3).
*, ° Values marked with the same symbol are statistically different ($p < 0.05$).

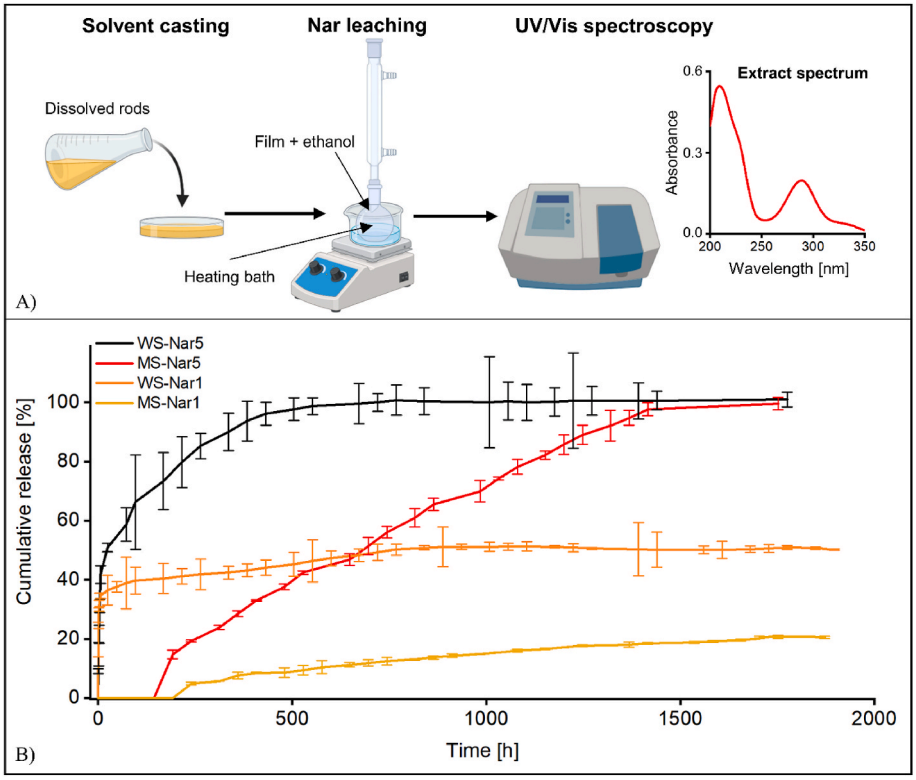

Fig. 5. Evaluation of Nar encapsulation efficiency (EE). (A) Schematic representation of the method employed for the measurement of Nar EE and representative UV spectrum of the Nar leached from MS-Nar rods; (B) Cumulative Nar release from the developed rods as a function of time (values reported as mean ± stand. dev, n = 3).

The EE of melt-spun rods was markedly lower than 100 % (Table 3), likely due to the loss of Nar into the extruder, corroborating the results reported in a previous study hypothesizing that the loading bioactive agent remained attached to the screw metal surface [45]. The hypothesis of Nar thermal degradation is unlikely, since its high thermal stability as shown by TGA and DSC analysis (Fig. 3), as well as by UV spectroscopy analysis (Fig. 5A). Indeed Nar spectra before and after extrusion were overlapped, being characterized by two absorption bands, one centered at 289 cm^{-1} with a shoulder at around 325 cm^{-1}, and the other one centered at 210 cm^{-1} characteristic of the flavonoid [46], without any signal related to Nar degradation products. In the case of wet-spun rods, the limited values of EE were probably due to drug diffusion into the coagulation bath, made of EtOH which is a good solvent for Nar.

Both in the case of melt- and wet-spun rods, an increase in the starting Nar concentration (1 or 5 wt%) led to a significant increase of EE and therefore a smaller difference between the theoretical and actual DL values (Table 3). This result could be related to different aspects, such as an effect of Nar concentration on polymer coagulation kinetics, as previously discussed, which can be a critical factor influencing Nar dissolution in EtOH during extrusion. In any case, other studies have previously shown that EE is directly related to the concentration of loaded active ingredients [47,48]. Moreover, no significant differences in terms of EE and L were detected by comparing samples fabricated by using different techniques but the same starting Nar concentration. Considering that a 6 mm length melt-spun insert (diameter of around 0.5 mm) has a mass of 3.3 ± 0.4 mg (n = 5), the Nar dose of a single implant would be 16.4 or 114.8 μg in the case of MS-Nar1 or MS-Nar5, respectively. In the case of wet-spun rods, the different EE values should be considered to reach the same injection dose, requiring multiple rods due to their micronized size. For instance, in the case of WS-Nar5 rods a mass of around 2.6 mg is required to have the same dose of an MS-Nar5 rod.

3.5. Nar release kinetics

Release kinetics of Nar from the developed rods was investigated through sample incubation in PBS 0.1 M at 37 °C, under orbital shaking, taking into account Nar solubility in these conditions (35.9 mg/L). The relevant cumulative Nar release curves are reported in Fig. 5B. The release rate of WS-Nar5 rods was high in the first hours (burst effect), reaching a 51 ± 2 % cumulative release in the first day. After that, drug release continued more slowly but consistently, reaching about a 100 % cumulative release after 38 days. In the case of MS-Nar5 rods, drug release was detected only after the first week, and then Nar concentration in the incubation medium increased steadily until a roughly 100 % cumulative release was reached after 73 days. This difference in drug release kinetics is probably due to the different dimensions and surface roughness of the two kinds of developed rods, determining for the wet-spun ones a higher interface surface area with the aqueous medium. Also in the case of a theoretical Nar concentration of 1 wt%, wet-spun devices showed an initial burst release and melt-spun rods a delayed release. However, the total cumulative release was much more attenuated, reaching after 80 days a value of around 40 % in the case of wet-spun rods, and 20 % in the case of melt-spun rods. The obtained results are in agreement with previous studies demonstrating that a higher drug loading in a polymeric matrix typically determines a faster release rate [49].

Release kinetics curves of WS-Nar1, WS-Nar5, and MS-Nar1 rods are better fitted by an exponential curve with a first order profile [50], while that of MS-Nar5 rods can be fitted by a linear function after an initial time lag (Table 3). The main difference between the two kinetics is that the first one involves a concentration-dependent release rate while the second one a constant release rate [51]. For this reason, devices presenting a zero order release kinetics are usually preferred because they are suitable to tailor drug release rate to the rate of drug elimination from the body. The result is a roughly constant drug concentration in the physiological medium at an effective but not toxic level, thereby minimizing adverse effects and improving patient compliance.

3.6. In vitro biological characterization of Nar-loaded rods on microglia cells

The anti-inflammatory effect of the WS-Nar5 rods was evaluated by monitoring the expression of pro-inflammatory markers by microglia cells. This device was selected since it was characterized by the fastest drug release rate, allowing to optimize short-term *in vitro* tests. The sterility of the rods was guaranteed by the fact that they were produced in EtOH and then kept into sterile Petri dishes. All the biological tests were carried out using the corresponding unloaded sample (WS-Nar0) as a control. The inflammatory effect on microglia cells was generated employing a lipopolysaccharide (LPS), which is an essential component of the bacterial cell wall of several Gram-negative bacteria and thus stimulates a strong inflammatory response in eucaryotic cells. The amount of device added to the culture medium (28.8 mg/10 mL) was calculated considering the release kinetics, with the aim of obtaining, after 24 h of incubation, a 60 μM Nar concentration, value previously reported to have an anti-inflammatory effect on microglia cells [28]. To this purpose we used both the murine BV2 microglia cell line and microglia primary cells isolated by post-natal day 1/2 (P1/P2) mice.

In a first kind of experiment, the WS-Nar5 rods were incubated for 24 h in growth medium and, after removal of the rods by centrifugation, the anti-inflammatory activity of the released Nar was evaluated by administrating this Nar-containing growth medium to BV2 cells and to microglia primary cells for 6 h, after which LPS was added for further 18 h. RTqPCR analysis showed that the presence of Nar released by the rods induces a significant decrease of the expression of the pro-inflammatory genes IL-1β, iNOS, and CCL2, which are up-regulated by LPS in cells treated with the medium incubated with the control rods (WS-Nar0). Histograms relevant to genes expression measured on BV2 cells cultured with medium previously treated with control rods WS-Nar0 or Nar-loaded rods WS-Nar5 are reported in Fig. 6A. Moreover, it was observed that the Nar released by the rods led to a significant increase of the CD206 transcript levels, characteristic of the anti-inflammatory phenotype (Fig. 6A). Analogous effects were reported when the same experiment was performed on primary microglia cells; the Nar released by the rods induced a down-regulation of IL-1β, IL-6, TNFα, iNOS, and CCL2 genes, and an up-regulation of CD206 (Fig. 6B). These results demonstrate that, after wet-spinning and polymer encapsulation, Nar preserves its activity in counteracting the pro-inflammatory phenotype induced by LPS in both BV2 and primary microglia cells.

In a second type of experiment, the WS-Nar5 rods were incubated for 24 h in growth medium, after which the growth medium containing the WS-Nar5 rods was administered to BV2 cells for 6 h and, subsequently, LPS was added for further 18 h. It was observed that BV2 cells tend to detach from the bottom of the Petri dish and to adhere to the surface of the rods (Fig. 7A). Cell detachment from the dish surface occurs in all areas of the cell plate and was more pronounced where the rods randomly accumulated; in such areas the dish surface was almost completely free of cells and the cells were localized on the device. This phenomenon does not depend on the presence of Nar, indeed it happens upon both WS-Nar5 and WS-Nar0 rods incubation (Fig. 7A). Being the loss of cell adhesion typical of apoptotic cells, we wondered if rods would affect cell viability, and, in order to clarify this issue, we evaluated the extent of apoptosis only in BV2 cells treated with WS-Nar0 rods; in fact, detachment of cells is independent on the presence of Nar into the device. We performed immunofluorescence of cleaved active caspase 3 (Cl Casp 3) and we realized the analysis of Cl Casp 3 fluorescence was difficult due to the auto-fluorescence of rods which interferes with the distinct detection of Cl Casp 3 fluorescence, especially for cells attached to the surface of the rods (Fig. 7B). However, besides the strong auto-fluorescence of the device, this figure shows that only few cleaved Casp3-positive apoptotic cells (Fig. 7B; white arrows) are present on the

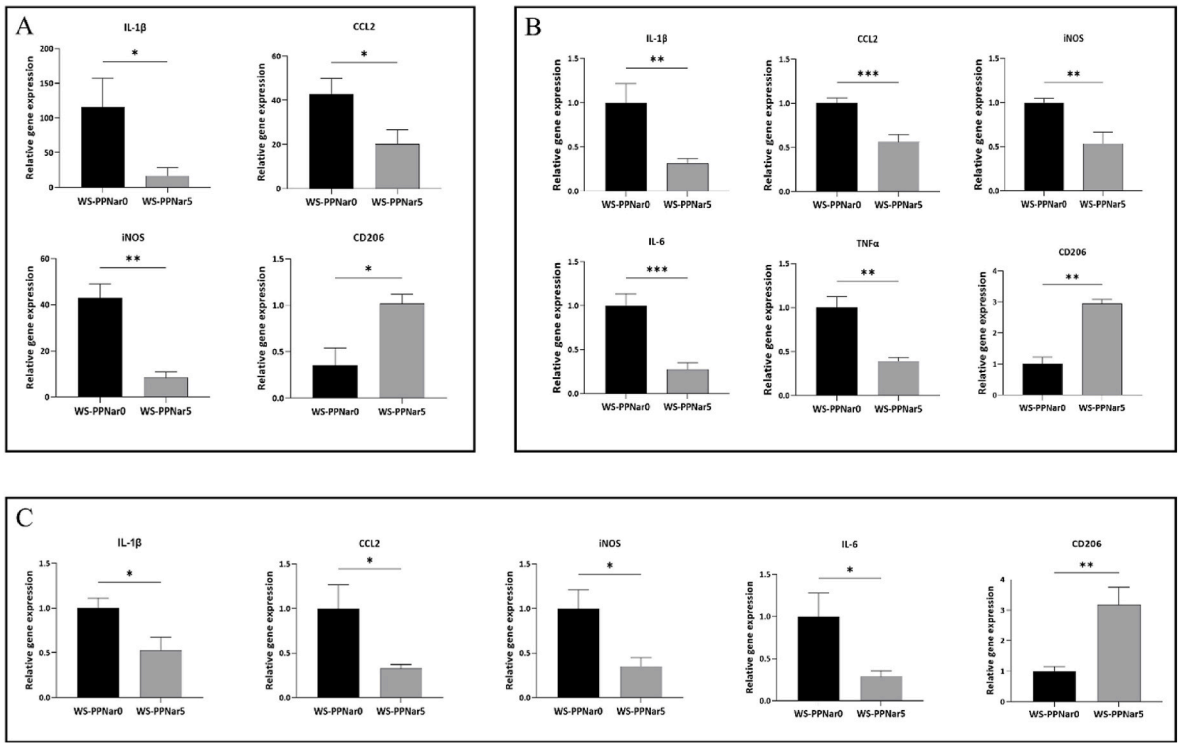

Fig. 6. Anti-inflammatory activity of WS-Nar5 rods. The mRNA levels were evaluated by qPCR on (A) BV2 microglia cells and on (B) microglia primary cells both of them pre-treated for 6 h with a culture medium obtained upon 24 h of WS-Nar0 (unloaded control rods) or WS-Nar5 incubation into growth medium. (C) qPCR on microglia primary cells pre-treated for 6 h with growth medium containing WS-Nar0 or WS-Nar5 after 24 h of incubation on a wheel. Cells were then exposed to LPS for further 18 h. Asterisks denote significance; *p ≤ 0.05, **p ≤ 0.01 and ***p ≤ 0.001 by unpaired Student's t-test.

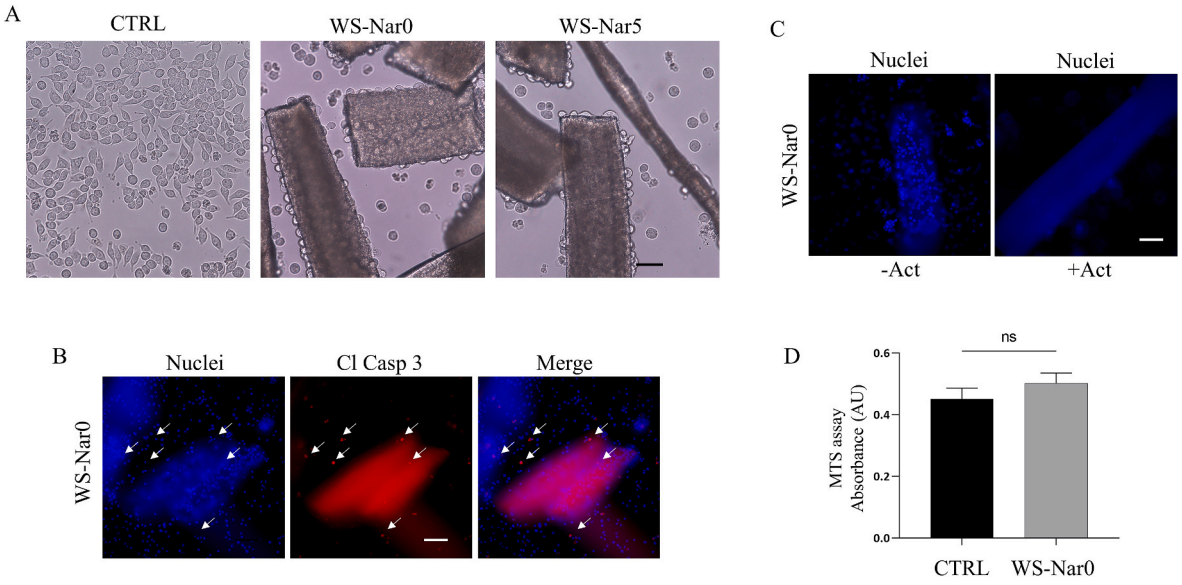

Fig. 7. Binding of BV2 cells to rods and assessment of apoptosis and cell survival. (A) Bright field images of BV2 microglia cells untreated (CTRL) or treated with WS-PPNar0/5. (B) Indirect immunostaining for Cl Casp 3 (red) of BV2 cells treated with WS-PPNar0 as in A. White arrows highlight examples of Cl Casp3-positive apoptotic cells. The large blurry shapes are due to the autofluorescence of the rods (both in red and blue). (C) BV2 cells incubated with WS-Nar0 as in B were un-treated (-Act) or treated (+Act) with Actinomycin 20 μM for further 6 h before immunostaining for Cl Casp 3 (red). DAPI was used to visualize all nuclei (blue). The large blurry shape is due to the autofluorescence of the rods. Scale bar: 100 μm. (D) MTS assay on BV2 microglia cells untreated (CTRL) or treated with WS-PPNar0 for 24 h. MTS was performed on the same number of CTRL and WS-PPNar0-treated cells which were counted for this purpose. Not significant (n.s.) by unpaired Student's t-test. (For interpretation of the references to color in this figure legend, the reader is referred to the Web version of this article.)

total number of cells (Fig. 7B; DAPI/nuclei). Moreover, we treated 24 h WS-Nar0-incubated BV2 cells with Actinomycin D - a transcription inhibitor acting as apoptotic inducer - and we observed that apoptotic BV2 cells completely detached from the dish and also from the device (see micrographs in Fig. 7C; +Act). By contrast, WS-Nar0-incubated BV2 cells not treated with Actinomycin D remained attached to device (Fig. 7C; Act^{-}), thus further demonstrating that cells on the surface of the devices were alive. To finally assess this issue, we performed the

MTS cell toxicity assay on both control cells and WS-Nar0-treated cells, and we did not observe any difference between these two conditions (Fig. 7D), further demonstrating the absence of rod toxicity. It is known that the migratory behavior of microglia cells is strongly influenced by substrate and extracellular matrix components [52]. In particular, it has been reported that PLGA particles are engulfed, therefore recognized, by macrophages although their effect on these cell activation is highly dependent on particles size [53]. Also, macrophages, therefore presumably microglia, might change polarization status depending on biomaterial features, such as size, geometry, hydrophobicity, and surface chemistry [54]. However, it is still not clear if microglia migration and recruitment by this device depend on the material or on the device surface morphology.

Differently from BV2 cells, primary microglia cells did not detach from the dish when incubated with WS-PPNar0/5 rods. Therefore, we could easier evaluate the extent of apoptosis in primary microglia cells through the immunofluorescent staining of active Cl Casp 3. As shown in Fig. 8, we confirmed that cells incubated with WS-PPNar0/5 rods are viable since there is not increase of active Cl Casp 3 staining or a higher number of picnotic nuclei compared to control cells where only a basal physiological apoptosis is observed. Since primary cells do not detach from the dish, we could collect them upon direct incubation with the device, extract RNA, and analyze gene expression. Fig. 6C shows that, also upon direct incubation, the WS-PPNar5 rods display an anti-inflammatory effect on LPS-treated primary microglia cells, compared to WS-PPNar0 rods.

4. Conclusion

A key result of this research activity was the development of novel protocols for the fabrication of Nar-loaded rods based on microbial PHBV blended with PLGA, as novel intravitreal implants. In particular, two types of rods were developed by means of optimized melt- and wet-spinning techniques. Both typologies of rods were loaded with two different concentrations of Nar (theoretical values of 1 and 5 wt%) obtaining an EE from 44 to 87 % in relationship to the fabrication technique and Nar loading. In addition, the different employed fabrication approaches resulted in rods with different dimensions (i.e., diameter and length), morphology (e.g., surface roughness), and thermal properties (e.g., crystallinity degree), as shown by SEM and DSC analysis. As a result, they demonstrated different Nar release kinetics when incubated in PBS at 37 °C. In particular, wet- and melt-spun rods loaded with a 1 wt% theoretical concentration of Nar showed a first order release kinetics, while MS-Nar5 rods showed a zero order release kinetics with a release rate roughly constant until reaching almost 100 % cumulative release after 73 days. WS-Nar5 rods showed an initial burst release phase (releasing 51 % of the encapsulated Nar in 24 h) followed by a sustained release with a decreasing rate up to 38 days when a total cumulative release was reached. Given this fast initial release allowing to optimize short-term *in vitro* biological investigations, this last kind of rods was tested for its anti-inflammatory properties by employing both murine BV2 and primary microglia cells treated with LPS. The anti-inflammatory activity of the WS-Nar5 rods was demonstrated by the decreased expression of the pro-inflammatory markers IL-1β, IL-6, CCL2, and iNOS compared to WS-Nar0 treated cells, and by the increased levels

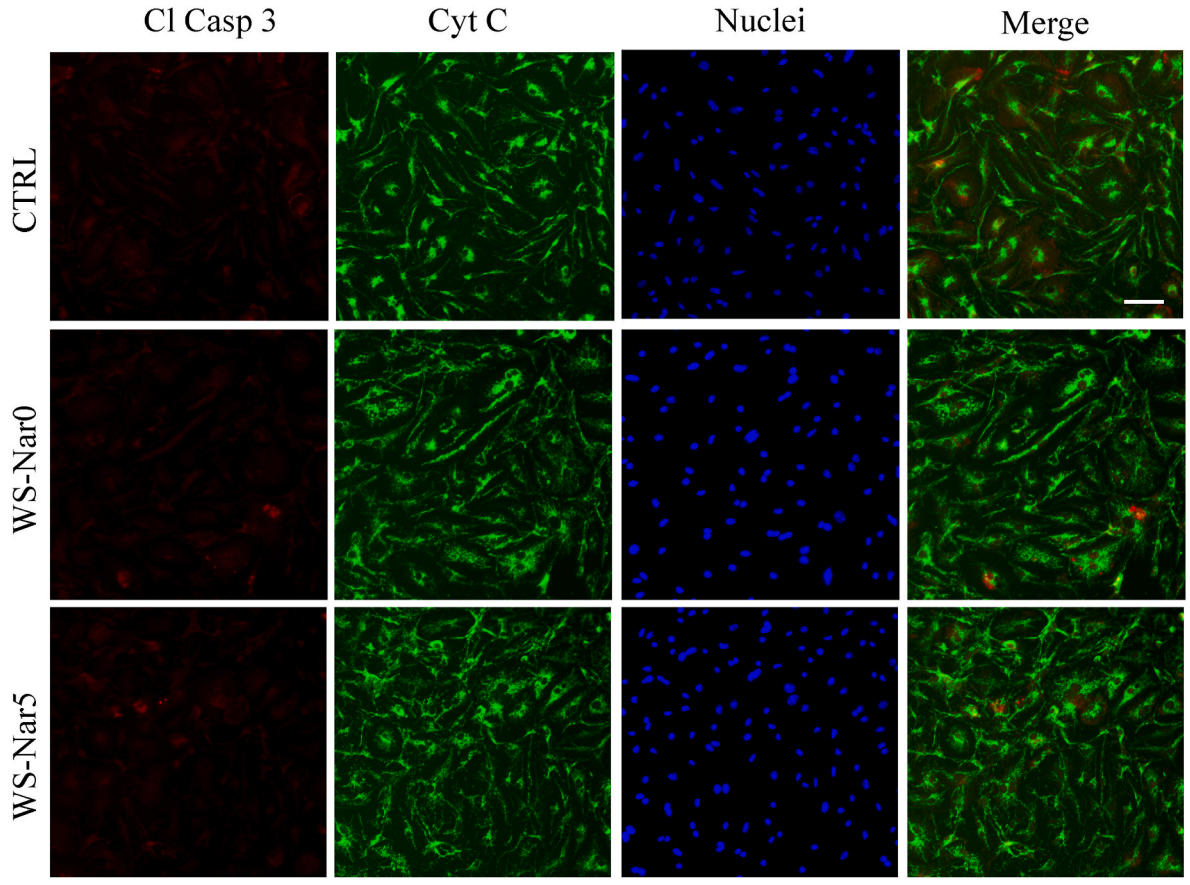

Fig. 8. Primary microglial cells incubated with rods do not undergo apoptosis. Primary microglial cells were untreated (CTRL) or pre-treated with WS-Nar0 or WS-Nar5 rods for 6 h and then administered with LPS for further 18 h before fixation and immunostaining for Cl Casp 3 (red) and Cyt C (green). Counterstaining with DAPI was used to visualize all nuclei (blue). Scale bar: 50 μm. (For interpretation of the references to color in this figure legend, the reader is referred to the Web version of this article.)

of the anti-inflammatory CD206 transcript. Moreover, these experiments revealed that microglia - the central nervous system macrophage cells - were attracted by the device and migrated from the plate to the rod surface, independently on the presence of Nar. The cytocompatibility of the device and the viability of the attached cells was also demonstrated.

Overall, these results suggest that an intravitreal implant based on a PHBV-PLGA blend loaded with the antioxidant molecule Nar could potentially be a therapeutic tool for the treatment of inflammation-induced ocular diseases. A natural progression of this study would therefore be the *in vivo* investigation of the developed rods for advanced intravitreal implantation and controlled drug release, as well as for other chronic inflammatory conditions.

Ethical approval

All animal procedures were conducted in accordance with European Guidelines for the use of animals in research (2010/63/EU), approved by the local ethics committee (Italian Ministry of Health-Direzione Generale della Sanità Animale e dei Farmaci Veterinari; Protocol Number 186/2022-PR) based on the requirements of Italian laws (the National Ethical Guidelines by Italian Ministry of Health; D. lgs. 26/2014) and conformed to ARRIVE guidelines 2.0 to improve the reporting of research involving animals. The investigators declare that the principle of the "3R" (replace, reduce, and refine) was carefully fulfilled.

CRediT authorship contribution statement

G. Pecorini: Writing – review & editing, Writing – original draft, Methodology, Investigation. **A. Votta:** Writing – original draft, Methodology, Investigation. **G. Tiralongo:** Writing – original draft, Investigation. **D. Volpi:** Investigation. **E. Ferraro:** Writing – review & editing, Writing – original draft, Supervision, Project administration, Methodology, Investigation, Funding acquisition, Conceptualization. **D. Puppi:** Writing – review & editing, Writing – original draft, Supervision, Project administration, Methodology, Investigation, Funding acquisition, Conceptualization.

Declaration of competing interest

The authors declare that they have no known competing financial interests or personal relationships that could have appeared to influence the work reported in this paper.

Data availability

Data will be made available on request.

Acknowledgments

This research was funded by the Ateneo Research Project (PRA) 2020—University of Pisa (Grant No. PRA_2020_37). The Centre for Instrumentation Sharing of the University of Pisa is acknowledged for SEM analysis and Randa Ishak for the relevant technical assistance. We also wish to thank Clotilde Lauro for the technical support concerning microglial primary cultures.

Appendix A. Supplementary data

Supplementary data to this article can be found online at https://doi.org/10.1016/j.jddst.2024.105895.

References

[1] B. Uttara, A. Singh, P. Zamboni, R. Mahajan, Oxidative stress and neurodegenerative diseases: a review of upstream and downstream antioxidant therapeutic options, Curr. Neuropharmacol. 7 (2009) 65–74, https://doi.org/10.2174/157015909787602823.
[2] N. Cuenca, L. Fernández-Sánchez, L. Campello, V. Maneu, P. De la Villa, P. Lax, et al., Cellular responses following retinal injuries and therapeutic approaches for neurodegenerative diseases, Prog. Retin. Eye Res. 43 (2014) 17–75, https://doi.org/10.1016/j.preteyeres.2014.07.001.
[3] A. Verkhratsky, M. Nedergaard, Astroglial cradle in the life of the synapse, Philos. Trans. R. Soc. Lond. B Biol. Sci. 369 (2014) 20130595, https://doi.org/10.1098/rstb.2013.0595.
[4] J.B. Lin, R.S. Apte, NAD(+) and sirtuins in retinal degenerative diseases: a look at future therapies, Prog. Retin. Eye Res. 67 (2018) 118–129, https://doi.org/10.1016/j.preteyeres.2018.06.002.
[5] P. Cao, C. Chen, A. Liu, Q. Shan, X. Zhu, C. Jia, et al., Early-life inflammation promotes depressive symptoms in adolescence via microglial engulfment of dendritic spines, Neuron 109 (2021) 2573–25789 e9, https://doi.org/10.1016/j.neuron.2021.06.012.
[6] T. Ishrat, I.N. Mohamed, B. Pillai, S. Soliman, A.Y. Fouda, A. Ergul, et al., Thioredoxin-interacting protein: a novel target for neuroprotection in experimental thromboembolic stroke in mice, Mol. Neurobiol. 51 (2015) 766–778, https://doi.org/10.1007/s12035-014-8766-x.
[7] B. dos Santos, C. dos Santos, J. Soares, K. Silva, J. Oliveira, G. Pereira, et al., The flavonoid agathisflavone directs brain microglia/macrophages to a neuroprotective anti-inflammatory and antioxidant state via regulation of NLRP3 inflammasom, Pharmaceutics 15 (2023), https://doi.org/10.3390/pharmaceutics15051410.
[8] M.M. Juca, F.M.S. Cysne Filho, J.C. de Almeida, D.D.S. Mesquita, J.R.M. Barriga, K. C.F. Dias, et al., Flavonoids: biological activities and therapeutic potential, Nat. Prod. Res. 34 (2020) 692–705, https://doi.org/10.1080/14786419.2018.1493588.
[9] J. Zhao, J. Yang, Y. Xie, Improvement strategies for the oral bioavailability of poorly water-soluble flavonoids: an overview, Int. J. Pharm. 570 (2019) 118642, https://doi.org/10.1016/j.ijpharm.2019.118642.
[10] D. Al-Dosari, M. Ahmed, S. Al-Rejaie, A. Alhomida, M. Ola, Flavonoid naringenin attenuates oxidative stress, apoptosis and improves neurotrophic effects in the diabetic rat retina, Nutrients 9 (2017) 1161, https://doi.org/10.3390/nu9101161.
[11] K. Shree Harini, D. Ezhilarasan, Flavonoids-based nanomedicines for the treatment of liver fibrosis: a recent progress, J. Drug Deliv. Sci. Technol. 93 (2024) 105467, https://doi.org/10.1016/j.jddst.2024.105467.
[12] A.M. Vargason, A.C. Anselmo, S. Mitragotri, The evolution of commercial drug delivery technologies, Nat. Biomed. Eng. 5 (2021) 951–967, https://doi.org/10.1038/s41551-021-00698-w.
[13] A. Vlachopoulos, G. Karlioti, E. Balla, V. Daniilidis, T. Kalamas, M. Stefanidou, et al., Poly(Lactic acid)-based microparticles for drug delivery applications: an overview of recent advances, Pharmaceutics 14 (2022), https://doi.org/10.3390/pharmaceutics14020359.
[14] S. Wachowiak, F. Danede, J.F. Willart, F. Siepmann, J. Siepmann, M. Hamoudi, PLGA implants for controlled dexamethasone delivery: impact of the polymer chemistry, J. Drug Deliv. Sci. Technol. 86 (2023) 104648, https://doi.org/10.1016/j.jddst.2023.104648.
[15] M. Pathak, A.G.A. Coombes, M. Jambhrunkar, D. Wang, K.J. Steadman, Evaluation of polycaprolactone matrices for sustained intravaginal delivery of a natural macromolecular microbicide, lactoferrin, J. Drug Deliv. Sci. Technol. 61 (2021) 101191, https://doi.org/10.1016/j.jddst.2019.101191.
[16] V. Kumar, N. Sharma, P. Janghu, R. Pasrija, M. Umesh, P. Chakraborty, et al., Synthesis and characterization of chitosan nanofibers for wound healing and drug delivery application, J. Drug Deliv. Sci. Technol. 87 (2023) 104858, https://doi.org/10.1016/j.jddst.2023.104858.
[17] K.N. How, W.H. Yap, C.L.H. Lim, B.H. Goh, Z.W. Lai, Hyaluronic acid-mediated drug delivery system targeting for inflammatory skin diseases: a mini review, Front. Pharmacol. 11 (2020) 1105, https://doi.org/10.3389/fphar.2020.01105.
[18] L. Wu, S.K. Kutas, B.R. Morrow, L. Hong, Sustained release of dipyridamole from collagen membranes, J. Drug Deliv. Sci. Technol. 80 (2023) 104180, https://doi.org/10.1016/j.jddst.2023.104180.
[19] M. Yekani, S. Maleki Dizaj, H. Sedaghat, J. Sadri Nahand, M. Saffari, M.Y. Memar, Preparation, biocompatibility, and antimicrobial effects of gelatin nanofibers scaffolds containing vancomycin and curcumin, J. Drug Deliv. Sci. Technol. 90 (2023) 105029, https://doi.org/10.1016/j.jddst.2023.105029.
[20] D. Puppi, G. Pecorini, F. Chiellini, Biomedical processing of polyhydroxyalkanoates, Bioengineering 6 (2019), https://doi.org/10.3390/bioengineering6040108.
[21] A. Rodriguez-Contreras, Recent advances in the use of polyhydroyalkanoates in biomedicine, Bioengineering 6 (2019), https://doi.org/10.3390/bioengineering6030082.
[22] M.L. Tebaldi, A.L.C. Maia, F. Poletto, F.V. de Andrade, D.C.F. Soares, Poly(-3-hydroxybutyrate-co-3-hydroxyvalerate) (PHBV): current advances in synthesis methodologies, antitumor applications and biocompatibility, J. Drug Deliv. Sci. Technol. 51 (2019) 115–126, https://doi.org/10.1016/j.jddst.2019.02.007.
[23] D. Puppi, F. Chiellini, Biodegradable polymers for biomedical additive manufacturing, Appl. Mater. Today 20 (2020) 100700, https://doi.org/10.1016/j.apmt.2020.100700.
[24] G. Pecorini, S. Braccini, G. Parrini, F. Chiellini, D. Puppi, Additive manufacturing of poly(3-hydroxybutyrate-co-3-hydroxyvalerate)/poly(D,L-lactide-co-glycolide) biphasic scaffolds for bone tissue regeneration, Int. J. Mol. Sci. 23 (2022), https://doi.org/10.3390/ijms23073895.
[25] H.M. Kim, S.J. Woo, Ocular drug delivery to the retina: current innovations and future perspectives, Pharmaceutics 13 (2021), https://doi.org/10.3390/pharmaceutics13010108.

[26] M.A. Costello, J. Liu, B. Chen, Y. Wang, B. Qin, X. Xu, et al., Drug release mechanisms of high-drug-load, melt-extruded dexamethasone intravitreal implants, Eur. J. Pharm. Biopharm. 187 (2023) 46–56, https://doi.org/10.1016/j.ejpb.2023.04.003.
[27] D. Puppi, F. Chiellini, Wet-spinning of biomedical polymers: from single-fibre production to additive manufacturing of three-dimensional scaffolds, Polym. Int. 66 (2017) 1690–1696, https://doi.org/10.1002/pi.5332.
[28] I. Piano, A. Votta, P. Colucci, F. Corsi, S. Vitolo, Cerri C. Chiara, et al., Anti-inflammatory reprogramming of microglia cells by metabolic modulators to counteract neurodegeneration; a new role for Ranolazine, Sci. Rep. 13 (2023) 20138, https://doi.org/10.1038/s41598-023-47540-8 in press.
[29] W. Kosorn, M. Sakulsumbat, P. Uppanan, P. Kaewkong, S. Chantaweroad, J. Jitsaard, et al., PCL/PHBV blended three dimensional scaffolds fabricated by fused deposition modeling and responses of chondrocytes to the scaffolds, J. Biomed. Mater. Res. B Appl. Biomater. 105 (2017) 1141–1150, https://doi.org/10.1002/jbm.b.33658.
[30] L. Belfiore, B. Aghaei, A.M.K. Law, J.C. Dobrowolski, L.J. Raftery, A.D. Tjandra, et al., Generation and analysis of 3D cell culture models for drug discovery, Eur. J. Pharmaceut. Sci. 163 (2021) 105876, https://doi.org/10.1016/j.ejps.2021.105876.
[31] A. Javadi, Y. Srithep, J. Lee, S. Pilla, C. Clemons, S. Gong, et al., Processing and characterization of solid and microcellular PHBV/PBAT blend and its RWF/nanoclay composites, Compos - A: Appl Sci Manuf 41 (2010) 982–990, https://doi.org/10.1016/j.compositesa.2010.04.002.
[32] M.A. Costello, J. Liu, Y. Wang, B. Qin, X. Xu, Q. Li, et al., Reverse engineering the Ozurdex dexamethasone intravitreal implant, Int. J. Pharm. 634 (2023) 122625, https://doi.org/10.1016/j.ijpharm.2023.122625.
[33] M.A. Repka, S. Bandari, V.R. Kallakunta, A.Q. Vo, H. McFall, M.B. Pimparade, et al., Melt extrusion with poorly soluble drugs - an integrated review, Int. J. Pharm. 535 (2018) 68–85, https://doi.org/10.1016/j.ijpharm.2017.10.056.
[34] A. Kovalcik, L. Sangroniz, M. Kalina, K. Skopalova, P. Humpolicek, M. Omastova, et al., Properties of scaffolds prepared by fused deposition modeling of poly (hydroxyalkanoates), Int. J. Biol. Macromol. 161 (2020) 364–376, https://doi.org/10.1016/j.ijbiomac.2020.06.022.
[35] N. Jacquel, C. Lo, H. Wu, Y. Wei, S. Wang, Solubility of polyhydroxyalkanoates by experiment and thermodynamic correlations, AIChE J. 53 (2007) 2704–2714, https://doi.org/10.1002/aic.11274.
[36] D. Puppi, A. Pirosa, G. Lupi, P.A. Erba, G. Giachi, F. Chiellini, Design and fabrication of novel polymeric biodegradable stents for small caliber blood vessels by computer-aided wet-spinning, Biomed. Mater. 12 (2017) 035011, https://doi.org/10.1088/1748-605X/aa6a28.
[37] C. Chou, J. Huang, C. Wu, C. Lee, C. Lin, Lengthening the polymer solidification time to improve the performance of polymer/ZnO nanorod hybrid solar cells, Sol. Energy Mater. Sol. Cells 93 (2009) 1608–1612, https://doi.org/10.1016/j.solmat.2009.04.016.
[38] B. Smith, A. Alexander, The effect of additives on the process of crystallization II. Further studies on calcium sulphate, J. Colloid Interface Sci. 34 (1970).
[39] B. Dimzoski, I. Fortelný, M. Šlouf, A. Sikora, D. Michálková, Morphology evolution during cooling of quiescent immiscible polymer blends: matrix crystallization effect on the dispersed phase coalescence, Polym. Bull. 70 (2012) 263–275, https://doi.org/10.1007/s00289-012-0848-1.
[40] A. Barbieri, D. Prevosto, M. Lucchesi, D. Leporini, Static and dynamic density effects due to the finite length of polymer chains: a molecular-dynamics investigation, J Condens Matter Phys 16 (2004) 6609–6618, https://doi.org/10.1088/0953-8984/16/36/026.
[41] C.L. Jennings, T.D. Dziubla, D.A. Puleo, Combined effects of drugs and plasticizers on the properties of drug delivery films, J. Bioact. Compat Polym. 31 (2016) 323–333, https://doi.org/10.1177/0883911515627178.
[42] S. Lappe, D. Mulac, K. Langer, Polymeric nanoparticles – influence of the glass transition temperature on drug release, Int. J. Pharm. 517 (2017) 338–347, https://doi.org/10.1016/j.ijpharm.2016.12.025.
[43] J.C. Jeong, J. Lee, K. Cho, Effects of crystalline microstructure on drug release behavior of poly(epsilon-caprolactone) microspheres, J. Contr. Release 92 (2003) 249–258, https://doi.org/10.1016/s0168-3659(03)00367-5.
[44] A. Ghasemzadeh, A. Baghdadi, H. Jaafar, M.K. Swamy, P.E. Megat Wahab, Optimization of flavonoid extraction from red and Brown rice bran and evaluation of the antioxidant properties, Molecules 23 (2018), https://doi.org/10.3390/molecules23081863.
[45] R. Chamberlain, H. Windolf, S. Geissler, J. Quodbach, J. Breitkreutz, Precise dosing of pramipexole for low-dosed filament production by hot melt extrusion applying various feeding methods, Pharmaceutics 14 (2022), https://doi.org/10.3390/pharmaceutics14010216.
[46] A. Gonzalez Moreno, P. Prieto, M.C. Ruiz Delgado, E. Dominguez, A. Heredia, A. de Cozar, Structure, isomerization and dimerization processes of naringenin flavonoids, Phys. Chem. Chem. Phys. 23 (2021) 18068–18077, https://doi.org/10.1039/d1cp01161h.
[47] A. Hurtado-Benavides, D. Dorado, A. Sánchez-Camargo, Study of the fatty acid profile and the aroma composition of oil obtained from roasted Colombian coffee beans by supercritical fluid extraction, J. Supercrit. Fluids 113 (2016) 44–52, https://doi.org/10.1016/j.supflu.2016.03.008.
[48] L. Wang, M.P. Pileni, Encapsulation of zwitterionic Au nanocrystals into liposomes by reverse phase evaporation method: influence of the surface charge, Langmuir 32 (2016) 12370–12377, https://doi.org/10.1021/acs.langmuir.6b01132.
[49] T. Huang, Y. Wang, Y. Shen, H. Ao, Y. Guo, M. Han, et al., Preparation of high drug-loading celastrol nanosuspensions and their anti-breast cancer activities in vitro and in vivo, Sci. Rep. 10 (2020) 8851, https://doi.org/10.1038/s41598-020-65773-9.
[50] M. Bruschi, Mathematical models of drug release, in: M.L. Bruschi (Ed.), Strategies to Modify the Drug Release from Pharmaceutical Systems, Elsevier, 2015, pp. 63–86.
[51] M.L. Laracuente, M.H. Yu, K.J. McHugh, Zero-order drug delivery: state of the art and future prospects, J. Contr. Release 327 (2020) 834–856, https://doi.org/10.1016/j.jconrel.2020.09.020.
[52] E. Moghadam, N. Sonenberg, M. Packirisamy, MicrofluidicWound-Healing assay for ECM and microenvironment properties on microglia BV2 cells migration, Biosensors (2023), https://doi.org/10.3390/bios13020290, 103390/bios13020290 13.
[53] R. Nicolete, D.F.d. Santos, L.H. Faccioli, The uptake of PLGA micro or nanoparticles by macrophages provokes distinct in vitro inflammatory response, Int. Immunopharm. 11 (2011) 1557–1563, https://doi.org/10.1016/j.intimp.2011.05.014.
[54] J.E. Rayahin, R.A. Gemeinhart, Activation of macrophages in response to biomaterials, in: M. Kloc (Ed.), Macrophages: Origin, Functions and Biointervention, Springer International Publishing, Cham, 2017, pp. 317–351.